CMS Physics Analysis Summary

Contact: cms-pag-conveners-susy@cern.ch 2020/05/23

Search for top squark pair production in the dilepton final state using 137 fb^{-1} of proton-proton collision integrated luminosity at $\sqrt{s}$ = 13 TeV

The CMS Collaboration

Abstract

A search for supersymmetric partners of the top quark is presented in final states with two oppositely charged leptons (electrons or muons), jets identified as originating from b quarks, and missing transverse momentum. The search uses data from proton-proton collisions at $\sqrt{s} = 13$ TeV collected from 2016 to 2018 using the CMS detector, amounting to 137 fb^{-1} of integrated luminosity. Hypothetical signal events are efficiently separated from the dominant top-quark pair background with requirements on the significance of missing transverse momentum and transverse mass variables. No significant deviation is observed from the expected background. Exclusion limits are set in the context of simplified supersymmetric models with pair-produced top squarks. For top squarks decaying exclusively to a top quark and a neutralino, exclusion limits are placed at 95% confidence level on the mass of the lightest top squark up to 925 GeV and on the lightest neutralino up to 450 GeV. If the decay proceeds via an intermediate chargino, the exclusion limit at 95% confidence level of the lightest top squark reaches up to 850 GeV for neutralino masses below 420 GeV. For top squarks undergoing a cascade decay through charginos and sleptons, the mass limits reach up to 1.4 TeV for the top squark and up to 900 GeV for the lightest neutralino.

1 Introduction

The standard model (SM) of particle physics accurately describes the overwhelming majority of observed particle physics phenomena. Nevertheless, several open problems cannot be explained by the SM, such as the hierarchy problem, the need for fine tuning to explain the large difference between the electroweak and the Planck scale [1, 2], and the lack of a candidate particle that explains the nature of dark matter in cosmological and astrophysical observations [3, 4]. Supersymmetry (SUSY) [5–12] is a well-motivated extension of the SM that provides a technically natural [13, 14] solution to both of these problems, through the introduction of an additional symmetry between bosons and fermions. In SUSY models, large quantum loop corrections to the masses of the Higgs bosons, mainly produced by the top quark, are mostly cancelled by the one produced by its SUSY partner, the top squark, if their masses are close in value. Similar cancellations occur for other particles, resulting in a natural solution to the hierarchy problem. Furthermore, SUSY introduces a new quantum number, R-parity [15], that distinguishes between SUSY and SM particles. If R-parity is conserved, top squarks are produced in pairs and the lightest SUSY particle is stable, which if neutral provides a good candidate for dark matter. In particular, the lighter top squark mass eigenstate $\widetilde{\mathrm{t}}_1$ may be within the LHC energy reach if SUSY provides a natural solution to the hierarchy problem [16], thus strongly motivating searching for top squark production.

In this note, we present a search for top squark pair production in data from pp collisions collected at a center-of-mass energy of 13 TeV, corresponding to an integrated luminosity of 137 fb^{-1}, with the CMS detector at the LHC from 2016 to 2018. The search is performed in a final state with two leptons (electrons or muons), hadronic jets identified as originating from b quarks, and significant missing transverse momentum ($p_{\mathrm{T}}^{\mathrm{miss}}$). The large background from SM $\mathrm{t\bar{t}}$ events is reduced by several orders of magnitude through the use of specially designed transverse-mass variables [17, 18]. Residual SM backgrounds in the search regions are validated in data control samples orthogonal in selection to the signal regions.

Simplified models [19–21] of strong top squark pair production and different top squark decay modes are considered. Following the naming convention in Ref. [22], top squark decays to top quarks and neutralinos ($\widetilde{\chi}_1^0$, identified as LSPs) are described by the T2tt model (Fig. 1, left). In the T2bW model (Fig. 1, center), both top squarks decay via an intermediate chargino ($\widetilde{\chi}_1^{\pm}$) into a b quark, a W boson, and an LSP. In both models, the undetected LSPs and the neutrinos from the leptonic W decays account for significant $p_{\mathrm{T}}^{\mathrm{miss}}$, and the leptons provide a final state with low SM backgrounds. In the T8bb$\ell\ell\nu\nu$ model (Fig. 1, right), both top squarks decay via an intermediate chargino to a b quark, a slepton, and a neutrino. This decay is assumed to be identical for all three flavors. The subsequent decay of the sleptons to neutralinos and leptons leads to a final state with the same particle content as in the T2tt model, albeit without a reduction of the signal acceptance from the leptonic W branching ratio.

Searches based on T2tt, T2bW, and T8bb$\ell\ell\nu\nu$ models using 8 and 13 TeV pp collision data were published by the CMS [23–29] and the ATLAS [30–38] experiments, with a $\widetilde{\mathrm{t}}_1$ mass excluded up to 1200 GeV in the T2tt model. In the T2bW and T8bb$\ell\ell\nu\nu$ models, top squarks with masses up to 1150 GeV and 1.3 TeV are excluded, respectively. The search presented in this note extends the previous result [28] by adding data collected in 2017 and 2018. Additonally, new methods are employed to suppress the main SM backgrounds.

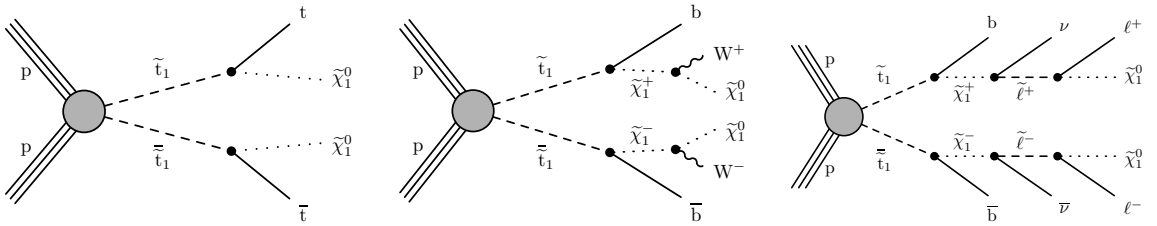

Figure 1: Diagrams for simplified SUSY models with strong production of top squark pairs $\tilde{t}_1\bar{\tilde{t}}_1$. In the T2tt model (left), the top squark decays to a top quark and a $\tilde{\chi}_1^0$. In the T2bW model (center), the top squark decays into a b quark and an intermediate $\tilde{\chi}_1^\pm$ that further decays into a W boson and a $\tilde{\chi}_1^0$. The decay of the intermediate $\tilde{\chi}_1^\pm$ to a slepton $\tilde{\ell}^\pm$ that yields $\nu\tilde{\chi}_1^0$ and a $\ell^\pm$ from the virtual slepton decay is described by the T8bb$\ell\ell\nu\nu$ model (right).

2 The CMS detector

The central feature of the CMS apparatus is a superconducting solenoid of 6 m internal diameter, providing a magnetic field of 3.8 T. Within the solenoid volume are a silicon pixel and strip tracker, a lead tungstate crystal electromagnetic calorimeter (ECAL), and a brass and scintillator hadron calorimeter (HCAL), each composed of a barrel and two endcap sections. Forward calorimeters extend the pseudorapidity coverage provided by the barrel and endcap detectors that improve the measurement of the imbalance in transverse momentum. Muons are detected in gas-ionization chambers embedded in the steel flux-return yoke outside the solenoid. A more detailed description of the CMS detector, together with a definition of the coordinate system used and the relevant kinematic variables, can be found in Ref. [39].

3 Event samples

The search is performed using a data set collected by the CMS experiment during the 2016, 2017, and 2018 LHC running periods. Events are selected online by different trigger algorithms that require the presence of one or two leptons (electrons or muons). The majority of events are selected with dilepton triggers with thresholds at 17 GeV (muon) and 23 GeV (electron) on the leading lepton p_T and 8 GeV (muon) or 12 GeV (electron) on the subleading lepton p_T. Single lepton triggers with a 24 GeV threshold for muons and with a 27 GeV threshold for electrons (32 GeV in the years 2017 and 2018) improve the selection efficiency. The efficiency of this online selection is measured using observed events that are selected based on the presence of jets and requirements on the missing transverse momentum. Typical efficiencies range from 95 to 99%, depending on the momenta and pseudorapidities (η) of the two leptons and are accounted for by scale factors applied to simulated events.

Simulated samples matching the varying conditions for each data taking period are generated using Monte Carlo (MC) techniques. The top quark-antiquark pair production ($t\bar{t}$) and t and s-channel single top quark background processes are simulated at next-to-leading-order (NLO) using the POWHEG v2 [40–47] event generator, and are normalized to next-to-next-to-leading order (NNLO) cross sections including soft-gluon resummation for the hadronic cross-section at next-to-next-to-leading logarithmic (NNLL) accuracy [48]. Events with single top quarks produced in association with W bosons (tW) are simulated using POWHEG v1 [49] and normalized to the NNLO cross section [50, 51]. The $t\bar{t}H$ process is generated using POWHEG v2 at NLO [52]. Drell-Yan events, generated with up to four extra partons in the matrix element calculations with MADGRAPH5_aMC@NLO v2.3.3 and v2.4.2 [53] at leading order (LO), and

Table 1: Cross section normalization order, event generator, and perturbative order for each simulated background process.

Process	Cross section normalization	Event generator	Perturbative order
$t\bar{t}$, single-t	NNLO+NNLL	POWHEG v2	NLO
tW	NNLO	POWHEG v1	NLO
$t\bar{t}H$	NLO	POWHEG v2	NLO
Drell-Yan	NNLO	MADGRAPH5_aMC@NLO	LO
$t\bar{t}Z$, $t\bar{t}W$, tZq, $t\bar{t}\gamma^{(*)}$, VVV, VV, WZ	NLO	MADGRAPH5_aMC@NLO	NLO
tHW, tHq, tWZ	LO	MADGRAPH5_aMC@NLO	LO

the cross section is computed at NNLO [54]. The processes $t\bar{t}Z$, $t\bar{t}W$, tZq, $t\bar{t}\gamma^{(*)}$, and the triboson processes are generated using MADGRAPH5_aMC@NLO at NLO. The cross section of the $t\bar{t}Z$ process is computed at NLO in perturbative quantum chromodynamics (QCD) and electroweak accuracy [55, 56]. The diboson process with decays to two leptons and two neutrinos (VV) and the WZ process are simulated with up to one extra parton in the matrix element calculations, using MADGRAPH5_aMC@NLO at NLO. The tWZ, tHq and tHW processes are generated at LO with MADGRAPH5_aMC@NLO. These processes are normalized to the most precise available cross section, corresponding to NLO accuracy in most cases. A summary of the event samples is provided in Table 1.

Generated events are interfaced with PYTHIA v8.226 (8.230) [57] using the CUETP8M1 (CP5) tune [58–60] for 2016 (2017, 2018) samples to simulate the fragmentation, parton shower, and hadronization of partons in the initial and final states, along with the underlying event. NNPDF parton distribution functions (PDFs) at different perturbative orders in QCD are used in v3.0 [61] and v3.1 [62] for 2016 and 2017-18 samples, respectively. Double counting of the partons generated with MADGRAPH5_aMC@NLO and PYTHIA is removed using the MLM [63] and the FXFX [64] matching schemes for LO and NLO samples, respectively. The events are subsequently processed with a GEANT4-based simulation model [65] of the CMS detector.

The SUSY signal samples are generated with MADGRAPH5_aMC@NLO with up to two extra partons at LO precision, interfaced with PYTHIA v8.226 (8.230) using the CUETP8M1 (CP2) tune for 2016 (2017, 2018). For the T2tt and T2bW models, the top squark mass is varied from 150 to 1200 GeV and the mass of the LSP is scanned from 1 to 650 GeV. The mass of the chargino in the T2bW model is assumed to be equal to the mean of the masses of the top squark and the lightest neutralino. For the T8bb$\ell\ell\nu\nu$ model, the top squark mass is varied from 200 to 1600 GeV and the mass of the LSP is scanned from 1 to 1200 GeV. For the masses of the intermediate chargino in T8bb$\ell\ell\nu\nu$ model we assume $m_{\tilde{\chi}_1^+} = (m_{\tilde{t}_1} + m_{\tilde{\chi}_1^0})/2$. For the slepton mass, the three values $x = 0.95$, 0.50, 0.05 are chosen in $m_{\tilde{\ell}} = x\,(m_{\tilde{\chi}_1^+} - m_{\tilde{\chi}_1^0}) + m_{\tilde{\chi}_1^0}$. The production cross sections of signal samples are normalized to NNLO plus next-to-next-to-leading logarithmic (NNLL) accuracy [66–78], and the simulation of the detector response is performed using the CMS fast detector simulation [79, 80].

All simulated samples include the simulation of additional pp collisions in the same or adjacent bunch crossings (pileup), and are reweighted according to the observed distribution of the number of interactions per bunch crossing. An additional correction is applied to account for a mismatch of the simulated samples and the observed distribution of primary vertices in the 2018 running period.

4 Object and Event selection

Event reconstruction uses the CMS particle-flow (PF) algorithm [81] which provides an exclusive set of electron [82], muon [83], charged and neutral hadron, and photon candidates. These particles are defined with respect to the primary pp interaction vertex, which is the vertex with the largest value of summed physics-object p_T^2. Charged hadron candidates not originating from the selected primary vertex in the event are discarded from the list of reconstructed particles.

Electron candidates are reconstructed using tracking and ECAL information, by combining the clusters of energy deposits in the ECAL with Gaussian sum filter tracks [82]. The electron identification is performed using shower shape variables, track-cluster matching variables, and track quality variables. The selection is optimized to identify electrons from the decay of SM bosons while rejecting electron candidates originating from jets. To reject electrons originating from photon conversion inside the detector, electrons are required to have all possible hits in the innermost tracker layers and to be incompatible with any conversion-like secondary vertices. Identification of muon candidates is performed using the quality of the geometrical matching between the measurements of the tracker and the muon system [83]. In all three running periods, the selected lepton candidates are required to satisfy $p_T > 30(20)\,\text{GeV}$ for the leading (subleading) lepton and $|\eta| < 2.4$, and are required to be isolated. To obtain a measure for the lepton isolation a cone with radius $\Delta R = \sqrt{(\Delta\eta)^2 + (\Delta\phi)^2} = 0.2$ (where ϕ is azimuthal angle in radians) around the lepton at the event vertex is constructed for leptons with $p_T < 50\,\text{GeV}$. For higher values of p_T the radius is reduced to $\Delta R = \max(0.05, 10\,\text{GeV}/p_T)$. A lepton is isolated if the scalar p_T sum of photons and neutral and charged hadrons reconstructed by the PF algorithm within this cone is less than 20% of the lepton p_T, $I_{\text{mini}} < 0.2$. The contribution of neutral particles from pileup interactions is estimated following the method described in Ref. [82], and subtracted from the isolation sum. The remaining selection criteria applied to electrons, muons, and the reconstruction of jets and p_T^{miss} are described in Ref. [28]. Jets are clustered from PF candidates using the anti-kT algorithm with a distance parameter of $R = 0.4$, and are required to statisfy $p_T > 30$, $|\eta| < 2.4$ and quality criteria. A multivariate b tagging discriminator algorithm, DeepCSV [84], is used to identify jets arising from b quark hadronization and decay (b jets). The chosen "medium" working point has a mistag rate of approximately 1% for light flavor jets and a corresponding b tagging efficiency of approximately 70% depending on jet transverse momentum and pseudorapidity.

Scale factors are applied to simulated events to take into account differences between the observed and simulated lepton reconstruction, identification, and isolation, and b tagging efficiencies. Typical corrections are less than 1% per lepton and less than 10% per b-tagged jet.

5 Search strategy

We select events containing a pair of leptons with opposite charge. The invariant mass of the lepton pair is required to be greater than 20 GeV to suppress backgrounds with misidentified or nonprompt leptons from the hadronization of (heavy flavor) jets in multijet events. Events with additional leptons with $p_T > 15\,\text{GeV}$ and satisfying a looser isolation criterion of $I_{\text{mini}} < 0.4$ are rejected. Events with a same-flavor lepton pair that is consistent with SM Drell-Yan production are removed by requiring $|m_Z - m(\ell\ell)| > 15\,\text{GeV}$, where $m(\ell\ell)$ is the invariant mass of the dilepton system and m_Z is the mass of the Z boson. To further suppress Drell-Yan and other vector boson backgrounds, we require the number of jets (N_{jets}) to be at least two and, among them, the number of b-tagged jets ($N_{\text{b jets}}$) to be at least one.

We use the $p_{\mathrm{T}}^{\mathrm{miss}}$ significance, denoted as $\mathcal{S}$, to suppress events where detector effects and misreconstruction of particles from pileup interactions are the main source of reconstructed $p_{\mathrm{T}}^{\mathrm{miss}}$. In short, the $\mathcal{S}$ observable measures the compatibilty of the reconstructed $p_{\mathrm{T}}^{\mathrm{miss}}$ with the null hypothesis of zero genuine $p_{\mathrm{T}}^{\mathrm{miss}}$. The $\mathcal{S}$ observable follows a χ^2-distribution with two degrees of freedom for events with no genuine $p_{\mathrm{T}}^{\mathrm{miss}}$. Fig. 2 shows the distribution of $\mathcal{S}$ in a $\mathrm{Z} \to \ell\ell$ sample, requiring events with two same-flavor leptons with $|m_{\mathrm{Z}} - m(\ell\ell)| < 15\,\mathrm{GeV}$, $N_{\mathrm{jets}} \geq 2$ and $N_{\mathrm{b\ jets}} = 0$. The algorithm is described in [85] and provides stability of event selection efficiency for different pileup. We exploit this property by requiring $\mathcal{S} > 12$ in order to suppress the otherwise overwhelming Drell-Yan background in the same-flavor channel. We further reduce this background by placing a requirement on the angular separation of $\vec{p}_{\mathrm{T}}^{\mathrm{miss}}$ and the momenta of the leading (j_1) and subleading (j_2) jets in the azimuthal plane. These criteria reject a small background of Drell-Yan events with strongly mismeasured jets.

The event preselection is summarized in Table 2. The resulting event sample is dominated by events with top quark pairs that decay to the dilepton final state.

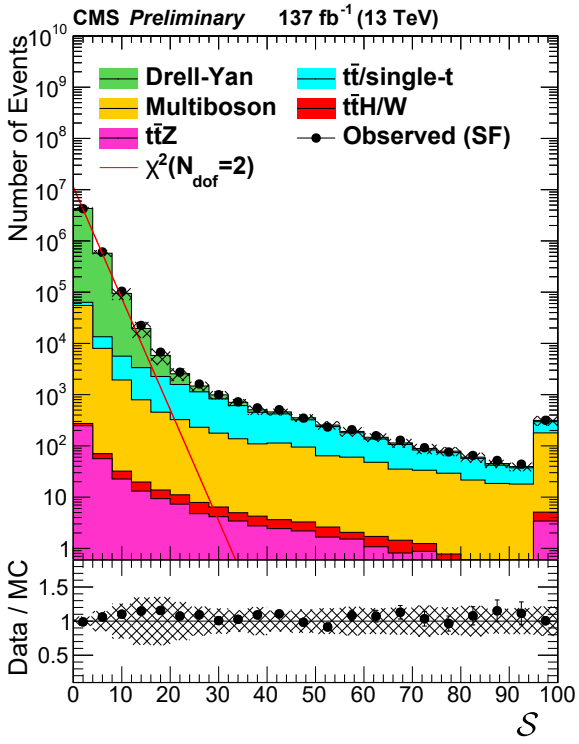

Figure 2: Distribution of $\mathcal{S}$ in a $\mathrm{Z} \to \ell\ell$ selection, requiring a same-flavor (SF) lepton pair. Events with no genuine $p_{\mathrm{T}}^{\mathrm{miss}}$ such as Drell-Yan follow a χ^2 distribution with two degrees of freedom (red line). Processes with true $p_{\mathrm{T}}^{\mathrm{miss}}$ such as $\mathrm{t\bar{t}}$ or production of two or more W or Z bosons populate high values of the $\mathcal{S}$ distribution.

The main search variable in this analysis is

$$M_{\mathrm{T2}}(\ell\ell) = \min_{\vec{p}_{\mathrm{T}}^{\mathrm{miss}\,1} + \vec{p}_{\mathrm{T}}^{\mathrm{miss}\,2} = \vec{p}_{\mathrm{T}}^{\mathrm{miss}}} \left(\max \left[M_{\mathrm{T}}(\vec{p}_{\mathrm{T}}^{\mathrm{vis}1}, \vec{p}_{\mathrm{T}}^{\mathrm{miss}1}), M_{\mathrm{T}}(\vec{p}_{\mathrm{T}}^{\mathrm{vis}2}, \vec{p}_{\mathrm{T}}^{\mathrm{miss}2}) \right] \right), \tag{1}$$

where the choice $\vec{p}_{\mathrm{T}}^{\mathrm{vis}1,2} = \vec{p}_{\mathrm{T}}^{\ell 1,2}$ corresponds to the definition introduced in Ref. [86]. The alternative choice $\vec{p}_{\mathrm{T}}^{\mathrm{vis}1,2} = \vec{p}_{\mathrm{T}}^{\ell 1,2} + \vec{p}_{\mathrm{T}}^{b1,2}$ involves the b-tagged jets and defines $M_{\mathrm{T2}}(\mathrm{b}\ell\mathrm{b}\ell)$. If only one b-tagged jet is found in the event, the jet with the highest p_{T} that does not pass the b-tagging

Table 2: Overview of the event selection requirements.

quantity	requirement
N_{leptons}	= 2 (e or μ), oppositely charged
$m(\ell\ell)$	$>$20 GeV
$\lvert m_{\text{Z}} - m(\ell\ell)\rvert$	$>$15 GeV, same flavor only
N_{jets}	$\geq$2
$N_{\text{b jets}}$	$\geq$1
$\mathcal{S}$	$>$12
$\cos\Delta\phi(p_{\text{T}}^{\text{miss}}, j_1)$	$<$0.80
$\cos\Delta\phi(p_{\text{T}}^{\text{miss}}, j_2)$	$<$0.96

selection is taken instead. The calculation of $M_{\text{T2}}(\ell\ell)$ and $M_{\text{T2}}(\text{b}\ell\text{b}\ell)$ is performed through the algorithm discussed in Ref. [87] assuming vanishing mass for the undetected particles and follows the description in Ref. [28]. The key feature of the $M_{\text{T2}}(\ell\ell)$ and $M_{\text{T2}}(\text{b}\ell\text{b}\ell)$ observables is that they retain a kinematic endpoint for background events even in the presence of two neutrinos from the leptonic decays of either two W bosons or two top quarks, respectively. In turn, signal events from the processes depicted in Fig. 1 are expected to populate the tails of these distributions.

Signal regions based on $M_{\text{T2}}(\ell\ell)$, $M_{\text{T2}}(\text{b}\ell\text{b}\ell)$ and $\mathcal{S}$ are defined to enhance sensitivity to different signal scenarios, listed in Table 3. The regions are further divided in different categories based on same- or different-flavor lepton pairs (SF and OF), accounting for the different SM background composition. The signal regions are defined so that there is no overlap between them, nor with the background-enriched control regions.

Table 3: Definition of the signal regions. The regions are further split into different- and same-flavor regions. The preselection in Table 2 is applied in all regions.

$M_{\text{T2}}(\text{b}\ell\text{b}\ell)$ (GeV)	$\mathcal{S}$	$100 < M_{\text{T2}}(\ell\ell) < 140$ GeV	$140 < M_{\text{T2}}(\ell\ell) < 240$ GeV	$M_{\text{T2}}(\ell\ell) > 240$ GeV
0–100	12–50	SR0	SR6	SR12
	$>$50	SR1	SR7	
100–200	12–50	SR2	SR8	
	$>$50	SR3	SR9	
$>$200	12–50	SR4	SR10	
	$>$50	SR5	SR11	

6 Background predictions

Events with an opposite-sign lepton pair are abundantly produced by Drell-Yan and $\text{t}\bar{\text{t}}$ processes. The event selection discussed in Sec. 4 efficiently rejects the vast majority of Drell-Yan events. Therefore, the major backgrounds from SM processes in the search regions are $\text{t}/\text{t}\bar{\text{t}}$ events that pass the $M_{\text{T2}}(\ell\ell)$ threshold because of severely mismeasured $p_{\text{T}}^{\text{miss}}$ or a misidentified lepton. In signal regions with large $M_{\text{T2}}(\ell\ell)$ and $\mathcal{S}$ requirements, $\text{t}\bar{\text{t}}\text{Z}$ events with $\text{Z} \to \nu\nu$ are the main SM background. Remaining Drell-Yan events with large $p_{\text{T}}^{\text{miss}}$ from mismeasurements, multiboson production and $\text{t}/\text{t}\bar{\text{t}}$ processes in association with a W, a Z or an H boson ($\text{t}\bar{\text{t}}\text{W}$, $\text{t}\bar{\text{t}}\text{H}$, tqZ) are sources of smaller contributions. The background estimation procedures and their corresponding control regions, listed in Table 4, are discussed in the following.

6.1 Top quark background

Events from the $\text{t}\bar{\text{t}}$ process are contained in the $M_{\text{T2}}(\ell\ell) < 100$ GeV region as long as the jets and leptons in each event are identified and their momenta are precisely measured. Three main

Table 4: Definition of control regions. The preselection in Table 2 is applied in all regions.

Name	Definition	
TTCRSF	$M_{T2}(\ell\ell) < 100$ GeV, SF leptons, $\lvert m(\ell\ell) - m_Z \rvert > 15\,\text{GeV}$	
TTCROF	$M_{T2}(\ell\ell) < 100$ GeV, OF leptons	
TTZ2j2b		$N_{\text{jets}} = 2$, $N_{\text{b jets}} \geq 2$
TTZ3j1b	$N_\ell = 3$, $\mathcal{S} \geq 0$, one SF lepton pair	$N_{\text{jets}} = 3$, $N_{\text{b jets}} = 1$
TTZ3j2b	with $\lvert m(\ell\ell) - m_Z \rvert < 15\,\text{GeV}$	$N_{\text{jets}} = 3$, $N_{\text{b jets}} \geq 2$
TTZ4j1b		$N_{\text{jets}} \geq 4$, $N_{\text{b jets}} = 1$
TTZ4j2b		$N_{\text{jets}} \geq 4$, $N_{\text{b jets}} \geq 2$
CR0-CR12	same as SR0-SR12 in Table 3, but SF leptons, $\lvert m(\ell\ell) - m_Z \rvert \leq 15\,\text{GeV}$ and $N_{\text{b jets}} = 0$	

sources are identified that promote $\mathrm{t\bar{t}}$ events into the tail of the $M_{T2}(\ell\ell)$ distribution. Firstly, the resolution of jet momenta are approximately Gaussian [88] and jet mismeasurements propagate to p_T^{miss}, which subsequently leads to values of $M_{T2}(\ell\ell)$ and $M_{T2}(\mathrm{b}\ell\mathrm{b}\ell)$ that do not obey the endpoint at the mother particle mass. For events with $M_{T2}(\ell\ell) \leq 140\,\text{GeV}$, this $\mathrm{t\bar{t}}$ component is dominant, while it amounts to less than 10% for signal regions with $M_{T2}(\ell\ell) > 140\,\text{GeV}$. Secondly, significant mismeasurements of the momentum of jets can be caused by the loss of photons and neutral hadrons showering in masked channels of the calorimeters, or neutrinos with high p_T within jets. The predicted rate and kinematic modeling of these rare non-Gaussian effects in the simulation are checked in a control region requiring same-flavor leptons satisfying $\lvert m(\ell\ell) - m_Z \rvert < 15\,\text{GeV}$. For $M_{T2}(\ell\ell) > 140\,\text{GeV}$, up to 50% of the top quark background falls into this category and its potential mismodeling is constrained by the good agreement of the simulated and observed p_T^{miss} distributions in the tail in this control region. No sign of unaccounted effects is observed, and we assign a 30% uncertainty to the yield of these events.

Thirdly, an electron or muon may fail the identification requirements, or the event may have a τ lepton produced in a W boson decay. If there is a nonprompt lepton from the hadronization of a b quark or a charged hadron misidentified as a lepton selected in the same event, the reconstructed value for $M_{T2}(\ell\ell)$ is not bound by the W mass. To validate the modeling of this contribution, we select events with one additional lepton satisfying loose isolation requirements on top of the selection in Table 2. In order to mimic the lost prompt lepton background, we recompute $M_{T2}(\ell\ell)$ by combining each of the isolated leptons with the extra lepton in both the observed and simulated samples. Since the transverse momentum balance is not significantly changed by lepton misidentification, the E_T^{miss} and $\mathcal{S}$ observables are not modified. Events with misidentified electrons or muons from this category constitute up to 40% of the top quark prediction for $M_{T2}(\ell\ell) > 140\,\text{GeV}$. We see good agreement between the observed and simulated kinematic distributions, indicating that simulation describes such backgrounds well and we assign an uncertainty of 50% to this contribution.

The $\mathrm{t\bar{t}}$ normalization is measured in-situ by including a signal-depleted control region defined by $M_{T2}(\ell\ell) < 100$ GeV in the signal extraction fit, yielding a scale factor for the $\mathrm{t\bar{t}}$ prediction of 1.02 ± 0.04. The region is split into the opposite-flavor (TTCROF) channel and the same-flavor channel (TTCRSF) where events with a Z boson candidate are rejected in the latter.

6.2 Top quark + X background

Top quarks produced in association with a boson ($t\bar{t}Z$, $t\bar{t}W$, $t\bar{t}H$, tqZ) form an irreducible background in decay channels where the boson decays to leptons or neutrinos. The $Z \to \nu\bar{\nu}$ decay in the $t\bar{t}Z$ process provides genuine p_T^{miss} and is the dominant background component at high values of $M_{T2}(\ell\ell)$. The decay mode $t\bar{t}Z \to (t \to b\ell^{\pm}\nu)(t \to bjj)(Z \to \ell^{\pm}\ell^{\mp})$ is used to measure the normalization of this contribution. The leading, subleading, and trailing lepton transverse momentum are required to satisfy thresholds of 40, 20, and 20 GeV, respectively. The invariant mass of the two same-flavor leptons with opposite charge is required to satisfy $|m(\ell\ell) - m_Z| < 10\,\text{GeV}$. The shape of the distribution of $p_T(Z)$ has recently been measured in the 2016 and 2017 data sets [89] and is well described by simulation. Five control regions requiring different N_{jets} and $N_{b\ jets}$ combinations are defined in Table 4 and labeled TTZ2j2b–TTZ4j2b. They are included in the signal extraction fit and the simulated number of $t\bar{t}Z$ events is scaled up by a factor of 1.22 ± 0.25, consistent with the initial prediction.

6.3 Drell-Yan and multiboson backgrounds

In order to measure the small residual Drell-Yan contribution that passes the event selection, we select dilepton events where we invert the Z boson veto, the b jet requirements, and remove the angular separation requirements on jets and $\vec{p}_T^{miss}$. We expect from the simulation that the selection will be dominated by Drell-Yan events and multiboson events. For each same-flavor signal region, we define a corresponding control region with the selections above and the signal region requirements on $M_{T2}(\ell\ell)$, $M_{T2}(b\ell b\ell)$, and $\mathcal{S}$. The regions are labeled CR0–CR12 in Table 4 and are included in the signal extraction fit. The Drell-Yan and multiboson background components are scaled up by 1.18 ± 0.28 and 1.35 ± 0.32, respectively.

The good modeling of the multiboson and $t\bar{t}$ processes, including potential sources of anomalous p_T^{miss}, is demonstrated in a validation region requiring $N_{jets} \geq 2$ and $N_{b\ jets} = 0$ and combining the same- and opposite-flavor channels. The observed distributions of the search variables are compared with the simulated distributions in Fig. 3. The hatched band includes the experimental systematic uncertainties and the uncertainties in the background normalizations. A 30% uncertainty is assigned on the contribution with non-Gaussian jet mismeasurements.

7 Systematic Uncertainties

Several experimental uncertainties affect the signal and background yield estimations. The efficiency of the trigger selection ranges from 95 to 99% with uncertainties lower than 2.3% in all signal and control regions. Offline lepton reconstruction and selection efficiencies are measured using $Z \to \ell\ell$ events in bins of lepton p_T and η. These measurements are performed separately in the observed and simulated data sets, with efficiency values ranging from 70 to 80%. Scale factors are used to correct the efficiencies measured in the simulated data to those in the observed data. The uncertainties in these scale factors are less than 3% per lepton and less than 5% in most of the search and control regions.

Uncertainties in the event yields resulting from the calibration of the jet energy scale are estimated by shifting the jet momenta in the simulation up and down by one standard deviation of the jet energy corrections. Depending on the jet p_T and η, the resulting uncertainty in the simulated yields from the jet energy scale is typically 4%, except in the lowest regions in $M_{T2}(\ell\ell)$ close to the m_W threshold where it can be as high as 20%. In addition, the energy scale of deposits from soft particles that are not clustered in jets are varied within their uncertainties and the resulting uncertainty reaches 7%. The b tagging efficiency in the simulation is corrected

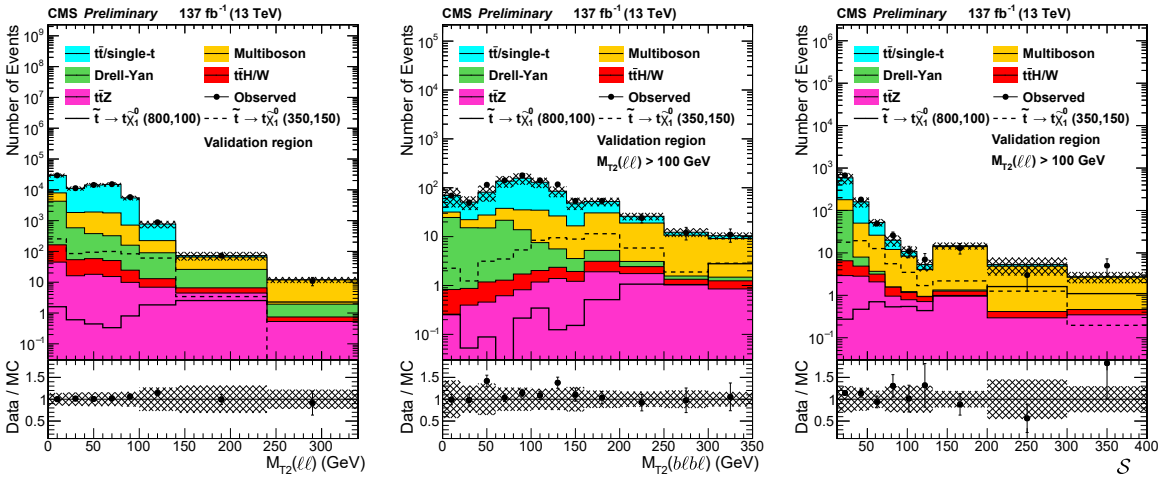

Figure 3: $M_{\mathrm{T2}}(\ell\ell)$, $M_{\mathrm{T2}}(\mathrm{b}\ell\mathrm{b}\ell)$ and $\mathcal{S}$ distributions in validation regions requiring $N_{\text{jets}} \geq 2$ and $N_{\text{b jets}} = 0$, combining the same- and opposite-flavor channel. All other event selection requirements are applied. For $M_{\mathrm{T2}}(\mathrm{b}\ell\mathrm{b}\ell)$ and $\mathcal{S}$, $M_{\mathrm{T2}}(\ell\ell) > 100\,\text{GeV}$ is required. The individual processes are scaled using their measured respective scale factors, as described in the text. The hashed band represents the experimental systematic uncertainties and the uncertainties in the scale factors as discussed in the text.

Table 5: Typical values (90% quantiles) and maximal values of the systematic uncertainties in all signal regions.

Systematic uncertainty	typical (%)	max (%)	Systematic uncertainty	typical (%)	max (%)
Integrated luminosity	2	2	Pileup modeling	5	7
Jet energy scale	4	20	Jet energy resolution	3	4
b tagging efficiency	2	3	b tagging mistage rate	1	7
Trigger efficiency	1	2	Modeling of unclustered energy	3	7
$t\bar{t}$ normalisation	9	9	Fake/non-prompt leptons	5	5
$t\bar{t}Z$ normalisation	10	14	Non-gaussian jet mismeasurements	6	6
Multiboson background normalisation	4	8	Rare background normalisation	5	8
Drell-Yan normalisation	3	8	Parton distribution functions	2	4
Lepton identification efficiency	3	5	μ_R and μ_F choice	7	11

using scale factors determined from the observed data [84], and uncertainties are propagated to all simulated events. These contribute an uncertainty of up to 3% in the predicted yields, depending on the p_{T} and η of the b-tagged jet.

The effect of all the experimental uncertainties described above is evaluated for each of the simulated processes in all signal regions, and is considered correlated across the analysis bins and simulated processes.

The uncertainties in the normalizations of the single top and top quark pair, $\mathrm{t\bar{t}Z}$, Drell-Yan, and multiboson backgrounds are discussed in Section 6. Finally, the uncertainty in the integrated luminosity is 2.3–2.5% [90–92].

Additional systematic uncertainties affect the modeling in simulation of the various processes, discussed in the following. Firstly, all simulated samples are reweighted according to the distribution of the true number of interactions at each bunch crossing. The uncertainty in the total inelastic pp cross section leads to uncertainties of 5% in the expected yields.

For the $\mathrm{t\bar{t}}$ and $\mathrm{t\bar{t}Z}$ backgrounds, we determine the event yield changes resulting from varying

the renormalization and factorization scales by a factor of 2 and 0.5, while keeping the overall normalization from the control region constant. We assign as the uncertainty the envelope of the considered yield variations, treated as uncorrelated between the background processes. Uncertainties in the PDFs can have a further effect on the simulated $M_{\mathrm{T2}}(\ell\ell)$ shape. We determine the change of acceptance in the signal regions using the PDF variations and assign the envelope of these variations—less than 4%—as a correlated uncertainty [93].

The contributions to the total uncertainty in the estimated backgrounds are summarised in Table 5, which provides the maximum uncertainties over all signal regions and the typical values, defined as the 90% quantile of the uncertainty values in all signal regions.

For the small contribution from top quark pair production in association with a W or a Higgs boson, we take an uncertainty of 20% in the cross section based on the variations of the generator scales and the PDFs.

Most of the sources of systematic uncertainty in the background estimates affect the prediction of the signal as well, and these are evaluated separately for each mass configuration of the considered simplified models. We further estimate the effect of missing higher-order corrections for the signal acceptance by varying the renormalization and factorization scales [94–96] and find that uncertainties are below 10%. The modeling of initial-state radiation (ISR) is relevant for the SUSY signal simulation in cases where the mass difference between the top squark and the LSP is small. The ISR reweighting is based on the number of ISR jets (N_j^{ISR}) so as to make the predicted jet multiplicity distribution agree with that observed. The same reweighting procedure is applied to SUSY Monte Carlo events and factors vary between 0.92 and 0.51 for N_j^{ISR} between 1 and 6. We take one half of the deviation from unity as the systematic uncertainty in these reweighting factors, correlated across search regions. It is generally found to have a small effect, but can reach 30% for compressed mass configurations. An uncertainty from potential differences of the modeling of $p_{\mathrm{T}}^{\mathrm{miss}}$ in the fast simulation of the CMS detector is evaluated by comparing the reconstructed $p_{\mathrm{T}}^{\mathrm{miss}}$ with the $p_{\mathrm{T}}^{\mathrm{miss}}$ obtained using generator-level information. This uncertainty ranges up to 20% and only affects the SUSY signal samples. For these samples, the scale factors and uncertainties for the tagging efficiency of b jets and leptons are evaluated separately. Typical uncertainties in the scale factors are below 2% for b-tagged jets, and between 1–7% for leptons.

8 Results

Good agreement between the predicted and observed $M_{\mathrm{T2}}(\ell\ell)$, $M_{\mathrm{T2}}(\mathrm{b}\ell\mathrm{b}\ell)$, and $\mathcal{S}$ distributions is found, as shown in Fig. 4. No significant deviation from the SM prediction is observed in any of the signal regions as shown in Fig. 5. The observed excess events in SR10SF are found to be close to the signal region selection thresholds. To perform the statistical interpretations, a likelihood function is formed with Poisson probability functions for all data regions, where the same-flavor and different-flavor signal regions are considered separately. The control and signal regions as depicted in Figs. 5 are included. The correlations of the uncertainties are taken into account as described in Section 7. A profile likelihood ratio in the asymptotic approximation [97] is used as test statistic. Upper limits on the production cross section are calculated at 95% confidence level (CL) using the asymptotic $\mathrm{CL_s}$ criterion [98, 99].

The results shown in Fig. 5 are interpreted in the context of simplified SUSY models of top squark production followed by a decay to top quarks and neutralinos (T2tt), via an intermediate chargino (T2bW), and via an additional interemediate slepton (T8bb$\ell\ell\nu\nu$). These interpretations are given in the $m_{\tilde{\mathrm{t}}_1}$–$m_{\tilde{\chi}_1^0}$ plane in Figs. 6 and 7. The color on the z axis indicates

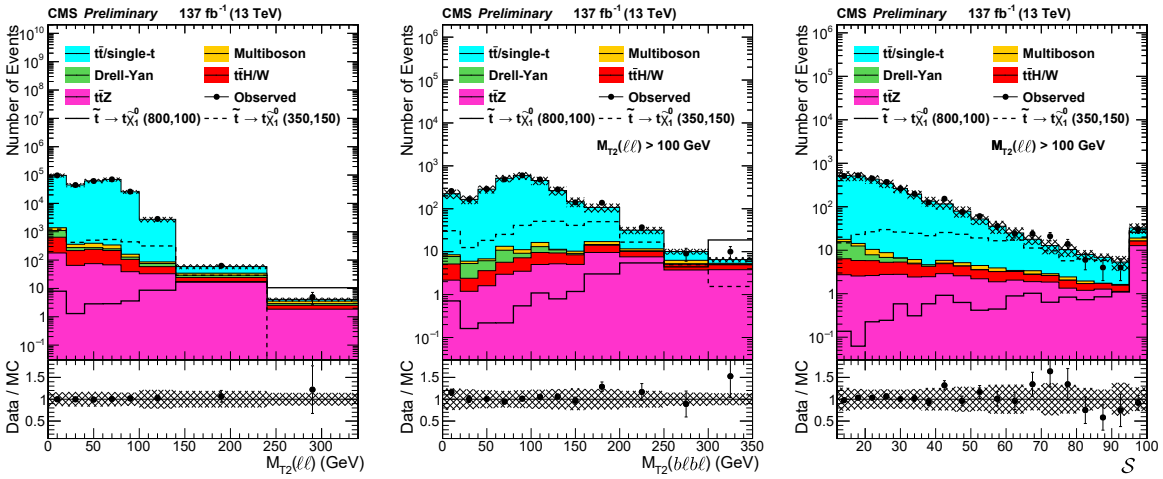

Figure 4: Distributions of $M_{T2}(\ell\ell)$ (left), $M_{T2}(b\ell b\ell)$ (middle), and $\mathcal{S}$ (right) for all lepton flavors for the selection defined in Table 2. Additionally, $M_{T2}(\ell\ell) > 100\,\text{GeV}$ is required for the $M_{T2}(b\ell b\ell)$ and $\mathcal{S}$.

the 95% CL upper limit on the cross section at each point in the $m_{\tilde{t}_1}$–$m_{\tilde{\chi}_1^0}$ plane. The area below the thick black curve represents the observed exclusion region at 95% CL assuming 100% branching fraction for the decays of the SUSY particles. The thick dashed red lines indicate the expected limit at 95% CL, while the region containing 68% of the distribution of limits expected under the background-only hypothesis is bounded by thin dashed red lines. The thin black lines show the effect of the theoretical uncertainties in the signal cross section. In the T2tt model we exclude mass configurations with $m_{\tilde{\chi}_1^0}$ up to 450 GeV and $m_{\tilde{t}_1}$ up to 925 GeV, assuming that the top quarks are unpolarized, thus improving by approximately 125 GeV in $m_{\tilde{t}_1}$ the results presented on a partial data set in Ref. [28]. The results for the T2bW is shown in Fig. 6 (right) and the results for T8bb$\ell\ell\nu\nu$ models are shown in Fig. 7. We exclude mass configurations with $m_{\tilde{\chi}_1^0}$ up to 420 GeV and $m_{\tilde{t}_1}$ up to 850 GeV in the T2bW model. The sensitivity in the T8bb$\ell\ell\nu\nu$ model strongly depends on the intermediate slepton mass and is largest when $x = 0.95$ in $m_{\tilde{\ell}} = x\,(m_{\tilde{\chi}_1^+} - m_{\tilde{\chi}_1^0}) + m_{\tilde{\chi}_1^0}$. In this case, excluded masses reach up to 900 GeV for $m_{\tilde{\chi}_1^0}$ and 1.4 TeV for $m_{\tilde{t}_1}$. These upper limits reduce to 750 GeV for $m_{\tilde{\chi}_1^0}$ and 1.3 GeV for $m_{\tilde{t}_1}$ when $x = 0.5$ and to 100 GeV for $m_{\tilde{\chi}_1^0}$ and 1.2 TeV for $m_{\tilde{t}_1}$ when $x = 0.05$.

9 Summary

A search for top squark pair production in final states with two leptons with opposite charge, b jets, and significant missing transverse momentum is presented. The data set of pp collisions corresponds to an integrated luminosity of 137 fb^{-1} is used that was collected with the CMS detector from 2016 to 2018 at a center-of-mass energy of 13 TeV. Transverse mass variables and the significance of missing transverse momentum are used to efficiently suppress backgrounds from SM processes. No evidence for a deviation from the expected background is observed, and results are interpreted in several simplified models for supersymmetric top squark pair production.

In the T2tt model with $\tilde{t}_1 \to t\tilde{\chi}_1^0$ decays, $\tilde{t}_1$ masses up to 925 GeV and $\tilde{\chi}_1^0$ masses up to 450 GeV are excluded. In the T2bW model with $\tilde{t}_1 \to b\tilde{\chi}_1^+ \to bW^+\tilde{\chi}_1^0$ decays, $\tilde{t}_1$ masses up to 850 GeV

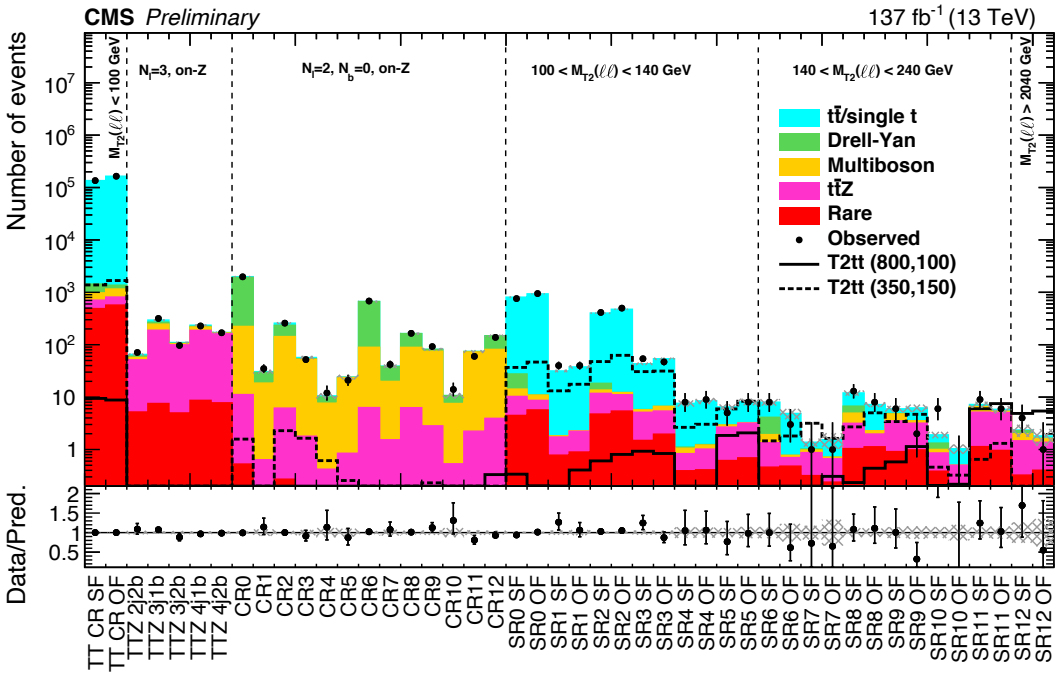

Figure 5: Predicted and observed yields in the signal and control regions as defined in Table 3 and 4. The control regions TTCRSF and TTCROF are defined by $M_{\mathrm{T2}}(\ell\ell) < 100\,\mathrm{GeV}$ and are used to constrain the $\mathrm{t\bar{t}}$ normalization. The $\mathrm{t\bar{t}Z}$ control regions employ a 3 lepton requirement in different N_{jets} and $N_{\mathrm{b\ jets}}$ bins. The dilepton invariant mass and $N_{\mathrm{b\ jets}}$ selections are inverted for CR0-CR12 in order to constrain the Drell-Yan and multiboson normalizations, using only the same-flavor channel. Good agreement between data and the post-fit SM prediction is observed in the control and signal regions. The hashed band reflects the post-fit systematic uncertainties.

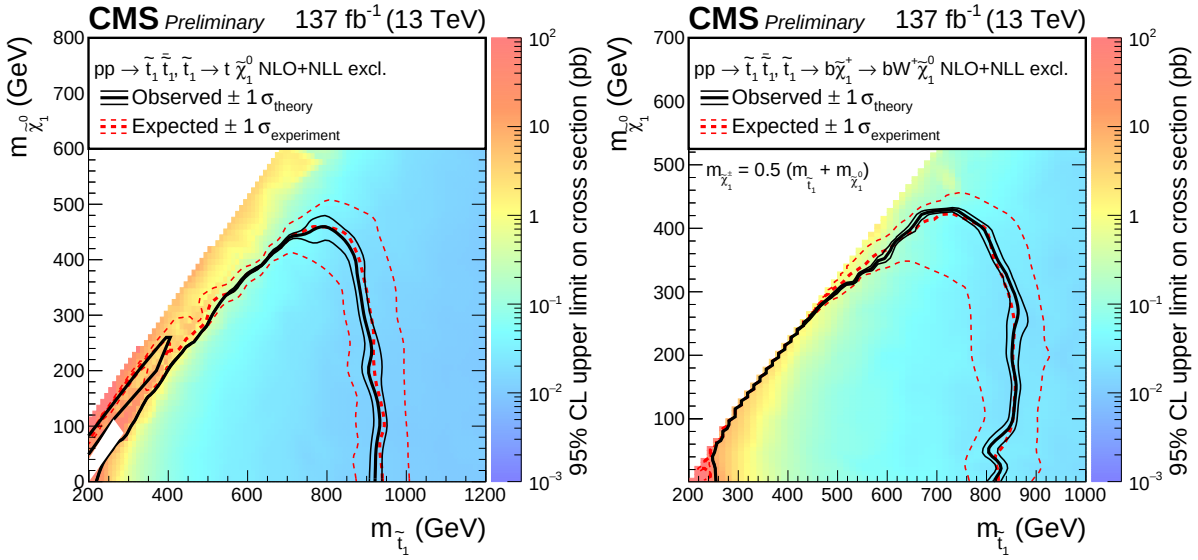

Figure 6: Expected and observed limits for the T2tt model with $\tilde{t}_1 \to t\tilde{\chi}_1^0$ decays (left) and for the T2bW model with $\tilde{t}_1 \to b\tilde{\chi}_1^+ \to bW^+\tilde{\chi}_1^0$ decays (right) in the $m_{\tilde{t}_1}$–$m_{\tilde{\chi}_1^0}$ mass plane. The color indicates the 95% CL upper limit on the cross section at each point in the plane. The area below the thick black curve represents the observed exclusion region at 95% CL assuming 100% branching fraction for the decays of the SUSY particles, while the dashed red lines indicate the expected limits at 95% CL and the region containing 68% of the distribution of limits expected under the background-only hypothesis. The thin black lines show the effect of the theoretical uncertainties in the signal cross section.

and $\tilde{\chi}_1^0$ masses up to 420 GeV are excluded, assuming the chargino mass to be the mean of the $\tilde{t}_1$ and the $\tilde{\chi}_1^0$ masses. In the T8bb$\ell\ell\nu\nu$ model with decays $\tilde{t}_1 \to b\tilde{\chi}_1^+ \to b\nu\tilde{\ell} \to b\nu\ell\tilde{\chi}_1^0$, and therefore 100% branching to dilepton final states, the sensitivity depends on the intermediate particle masses. With the chargino mass again taken as the mean of the $\tilde{t}_1$ and the $\tilde{\chi}_1^0$ masses, the strongest exclusion is obtained if the slepton mass is close to the chargino mass. In this case, excluded masses reach up to 1.4 TeV for $\tilde{t}_1$ and 900 GeV for $\tilde{\chi}_1^0$. When the slepton mass and the chargino mass are similar, these numbers reduce to 1.3 TeV for $\tilde{t}_1$ and 750 GeV for $\tilde{\chi}_1^0$. A further reduction to 1.2 TeV for $\tilde{t}_1$ and to 100 GeV for $\tilde{\chi}_1^0$ is observed when the slepton mass is close to the neutralino mass.

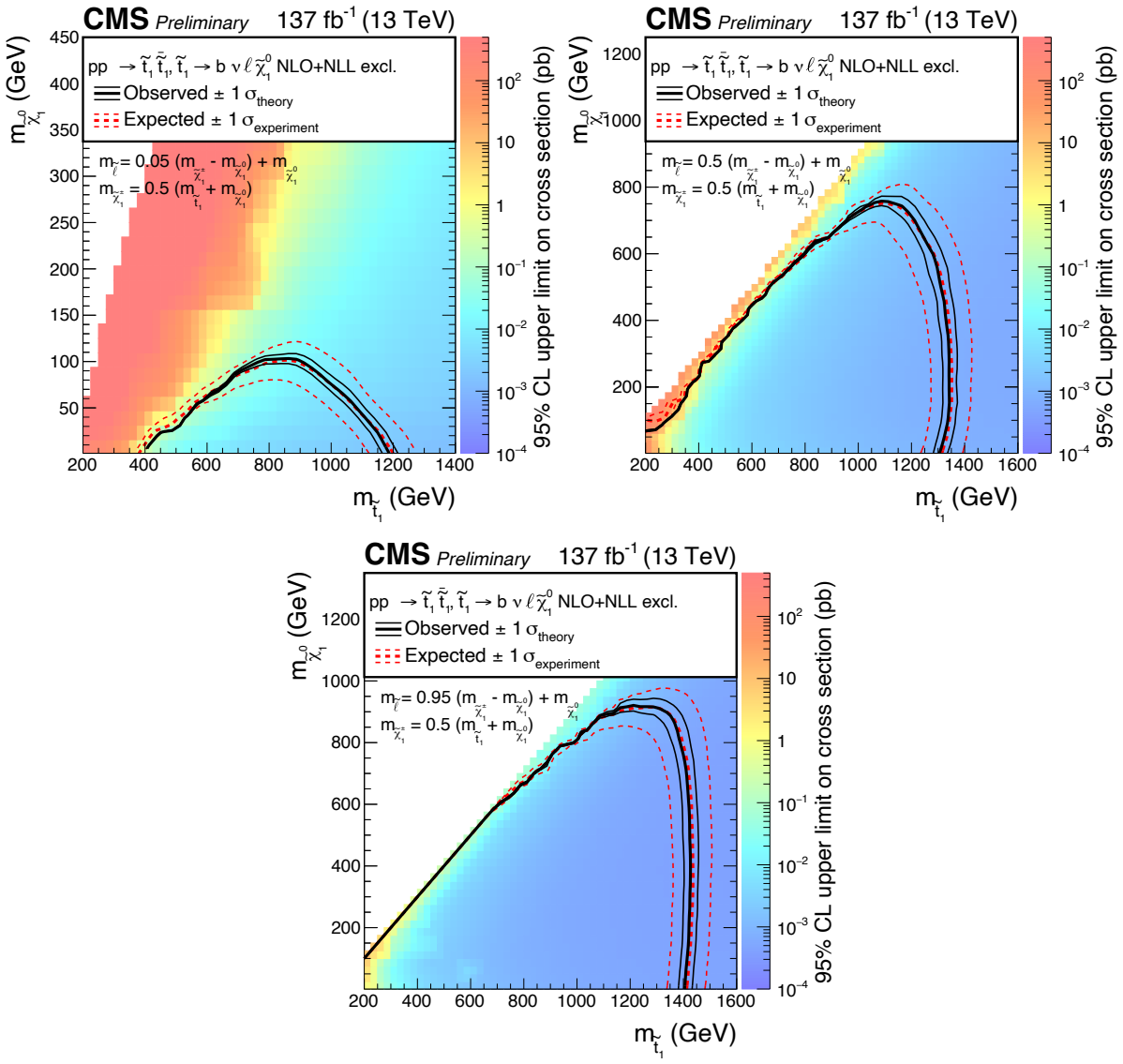

Figure 7: Expected and observed limits for the T8bb$\ell\ell\nu\nu$ model with $\tilde{t}_1 \to b\tilde{\chi}_1^+ \to b\nu\tilde{\ell} \to b\nu\ell\tilde{\chi}_1^0$ decays in the $m_{\tilde{t}_1}$–$m_{\tilde{\chi}_1^0}$ mass plane for three different mass configurations defined by $m_{\tilde{\ell}} = x\,(m_{\tilde{\chi}_1^+} - m_{\tilde{\chi}_1^0}) + m_{\tilde{\chi}_1^0}$ with $x = 0.05$ (upper left), $x = 0.5$ (upper right), and $x = 0.95$ (lower). The description of curves is the same as in the caption of Fig. 6.

References

[1] E. Witten, "Dynamical breaking of supersymmetry", *Nucl. Phys. B* **188** (1981) 513, doi:10.1016/0550-3213(81)90006-7.

[2] R. Barbieri and G. Giudice, "Upper Bounds on Supersymmetric Particle Masses", *Nucl. Phys. B* **306** (1988) 63–76, doi:10.1016/0550-3213(88)90171-X.

[3] G. Bertone, D. Hooper, and J. Silk, "Particle dark matter: Evidence, candidates and constraints", *Phys. Rept.* **405** (2005) 279–390, doi:10.1016/j.physrep.2004.08.031, arXiv:hep-ph/0404175.

[4] J. L. Feng, "Dark Matter Candidates from Particle Physics and Methods of Detection", *Ann. Rev. Astron. Astrophys.* **48** (2010) 495–545, doi:10.1146/annurev-astro-082708-101659, arXiv:1003.0904.

[5] P. Ramond, "Dual theory for free fermions", *Phys. Rev. D* **3** (1971) 2415, doi:10.1103/PhysRevD.3.2415.

[6] Y. A. Gol'fand and E. P. Likhtman, "Extension of the algebra of Poincaré group generators and violation of P invariance", *JETP Lett.* **13** (1971) 323.

[7] A. Neveu and J. H. Schwarz, "Factorizable dual model of pions", *Nucl. Phys. B* **31** (1971) 86, doi:10.1016/0550-3213(71)90448-2.

[8] D. V. Volkov and V. P. Akulov, "Possible universal neutrino interaction", *JETP Lett.* **16** (1972) 438.

[9] J. Wess and B. Zumino, "A lagrangian model invariant under supergauge transformations", *Phys. Lett. B* **49** (1974) 52, doi:10.1016/0370-2693(74)90578-4.

[10] J. Wess and B. Zumino, "Supergauge transformations in four dimensions", *Nucl. Phys. B* **70** (1974) 39, doi:10.1016/0550-3213(74)90355-1.

[11] P. Fayet, "Supergauge invariant extension of the Higgs mechanism and a model for the electron and its neutrino", *Nucl. Phys. B* **90** (1975) 104, doi:10.1016/0550-3213(75)90636-7.

[12] H. P. Nilles, "Supersymmetry, supergravity and particle physics", *Phys. Rep.* **110** (1984) 1, doi:10.1016/0370-1573(84)90008-5.

[13] S. Dimopoulos and H. Georgi, "Softly broken supersymmetry and SU(5)", *Nucl. Phys. B* **193** (1981) 150, doi:10.1016/0550-3213(81)90522-8.

[14] R. K. Kaul and P. Majumdar, "Cancellation of Quadratically Divergent Mass Corrections in Globally Supersymmetric Spontaneously Broken Gauge Theories", *Nucl. Phys. B* **199** (1982) 36, doi:10.1016/0550-3213(82)90565-X.

[15] G. R. Farrar and P. Fayet, "Phenomenology of the Production, Decay, and Detection of New Hadronic States Associated with Supersymmetry", *Phys. Lett.* **76B** (1978) 575–579, doi:10.1016/0370-2693(78)90858-4.

[16] M. Papucci, J. T. Ruderman, and A. Weiler, "Natural SUSY endures", *JHEP* **09** (2012) 035, doi:10.1007/JHEP09(2012)035, arXiv:1110.6926.

[17] J. Smith, W. L. van Neerven, and J. A. M. Vermaseren, "The transverse mass and width of the W boson", *Phys. Rev. Lett.* **50** (1983) 1738, doi:10.1103/PhysRevLett.50.1738.

[18] C. G. Lester and D. J. Summers, "Measuring masses of semiinvisibly decaying particles pair produced at hadron colliders", *Phys. Lett. B* **463** (1999) 99, doi:10.1016/S0370-2693(99)00945-4, arXiv:hep-ph/9906349.

[19] J. Alwall, P. Schuster, and N. Toro, "Simplified models for a first characterization of new physics at the LHC", *Phys. Rev. D* **79** (2009) 075020, doi:10.1103/PhysRevD.79.075020, arXiv:0810.3921.

[20] J. Alwall, M.-P. Le, M. Lisanti, and J. G. Wacker, "Model-independent jets plus missing energy searches", *Phys. Rev. D* **79** (2009) 015005, doi:10.1103/PhysRevD.79.015005, arXiv:0809.3264.

[21] LHC New Physics Working Group Collaboration, "Simplified models for LHC new physics searches", *J. Phys. G* **39** (2012) 105005, doi:10.1088/0954-3899/39/10/105005, arXiv:1105.2838.

[22] CMS Collaboration, "Interpretation of searches for supersymmetry with simplified models", *Phys. Rev. D* **88** (2013) 052017, doi:10.1103/PhysRevD.88.052017, arXiv:1301.2175.

[23] CMS Collaboration, "Search for top-squark pair production in the single-lepton final state in pp collisions at $\sqrt{s} = 8$ TeV", *Eur. Phys. J. C* **73** (2013) 2677, doi:10.1140/epjc/s10052-013-2677-2, arXiv:1308.1586.

[24] CMS Collaboration, "Search for direct pair production of scalar top quarks in the single- and dilepton channels in proton-proton collisions at $\sqrt{s} = 8$ TeV", *JHEP* **07** (2016) 027, doi:10.1007/JHEP07(2016)027, arXiv:1602.03169. [Erratum: doi:10.1007/JHEP09(2016)056].

[25] CMS Collaboration, "Searches for pair production of third-generation squarks in $\sqrt{s} = 13$ TeV pp collisions", *Eur. Phys. J. C* **77** (2017) 327, doi:10.1140/epjc/s10052-017-4853-2, arXiv:1612.03877.

[26] CMS Collaboration, "Search for top squark pair production in pp collisions at $\sqrt{s}$ = 13 TeV using single lepton events", *JHEP* **10** (2017) 019, doi:10.1007/JHEP10(2017)019, arXiv:1706.04402.

[27] CMS Collaboration, "Search for direct production of supersymmetric partners of the top quark in the all-jets final state in proton-proton collisions at $\sqrt{s} = 13$ TeV", *JHEP* **10** (2017) 005, doi:10.1007/JHEP10(2017)005, arXiv:1707.03316.

[28] CMS Collaboration, "Search for top squarks and dark matter particles in opposite-charge dilepton final states at $\sqrt{s} = 13$ TeV", *Phys. Rev. D* **97** (2018) 032009, doi:10.1103/PhysRevD.97.032009, arXiv:1711.00752.

[29] CMS Collaboration, "Search for direct top squark pair production in events with one lepton, jets, and missing transverse momentum at 13 TeV with the CMS experiment", *JHEP* **05** (2020) 032, doi:10.1007/JHEP05(2020)032, arXiv:1912.08887.

[30] ATLAS Collaboration, "ATLAS Run 1 searches for direct pair production of third-generation squarks at the Large Hadron Collider", *Eur. Phys. J. C* **75** (2015) 510, doi:10.1140/epjc/s10052-015-3726-9, arXiv:1506.08616. [Erratum: doi:10.1140/epjc/s10052-016-3935-x].

[31] ATLAS Collaboration, "Search for top squark pair production in final states with one isolated lepton, jets, and missing transverse momentum in $\sqrt{s} = 8$ TeV pp collisions with the ATLAS detector", *JHEP* **11** (2014) 118, doi:10.1007/JHEP11(2014)118, arXiv:1407.0583.

[32] ATLAS Collaboration, "Search for direct top-squark pair production in final states with two leptons in pp collisions at $\sqrt{s} = 8$ TeV with the ATLAS detector", *JHEP* **06** (2014) 124, doi:10.1007/JHEP06(2014)124, arXiv:1403.4853.

[33] ATLAS Collaboration, "Search for top squarks in final states with one isolated lepton, jets, and missing transverse momentum in $\sqrt{s} = 13$ TeV pp collisions with the ATLAS detector", *Phys. Rev. D* **94** (2016) 052009, doi:10.1103/PhysRevD.94.052009, arXiv:1606.03903.

[34] ATLAS Collaboration, "Search for direct top squark pair production in final states with two leptons in $\sqrt{s} = 13$ TeV pp collisions with the ATLAS detector", *Eur. Phys. J. C* **77** (2017) 898, doi:10.1140/epjc/s10052-017-5445-x, arXiv:1708.03247.

[35] ATLAS Collaboration, "Search for a scalar partner of the top quark in the jets plus missing transverse momentum final state at $\sqrt{s}$=13 TeV with the ATLAS detector", *JHEP* **12** (2017) 085, doi:10.1007/JHEP12(2017)085, arXiv:1709.04183.

[36] ATLAS Collaboration, "Search for top-squark pair production in final states with one lepton, jets, and missing transverse momentum using 36 fb^{-1} of $\sqrt{s} = 13$ TeV pp collision data with the ATLAS detector", *JHEP* **06** (2018) 108, doi:10.1007/JHEP06(2018)108, arXiv:1711.11520.

[37] ATLAS Collaboration, "Search for squarks and gluinos in final states with same-sign leptons and jets using 139 fb^{-1} of data collected with the ATLAS detector", arXiv:1909.08457.

[38] ATLAS Collaboration, "Search for a scalar partner of the top quark in the all-hadronic $t\bar{t}$ plus missing transverse momentum final state at $\sqrt{s}$=13 TeV with the ATLAS detector", arXiv:2004.14060.

[39] CMS Collaboration, "The CMS experiment at the CERN LHC", *JINST* **3** (2008) S08004, doi:10.1088/1748-0221/3/08/S08004.

[40] P. Nason, "A New method for combining NLO QCD with shower Monte Carlo algorithms", *JHEP* **11** (2004) 040, doi:10.1088/1126-6708/2004/11/040, arXiv:hep-ph/0409146.

[41] S. Frixione, P. Nason, and C. Oleari, "Matching NLO QCD computations with Parton Shower simulations: the POWHEG method", *JHEP* **11** (2007) 070, doi:10.1088/1126-6708/2007/11/070, arXiv:0709.2092.

[42] S. Alioli, P. Nason, C. Oleari, and E. Re, "A general framework for implementing NLO calculations in shower Monte Carlo programs: the POWHEG BOX", *JHEP* **06** (2010) 043, doi:10.1007/JHEP06(2010)043, arXiv:1002.2581.

[43] J. M. Campbell, R. K. Ellis, P. Nason, and E. Re, "Top-Pair Production and Decay at NLO Matched with Parton Showers", *JHEP* **04** (2015) 114, doi:10.1007/JHEP04(2015)114, arXiv:1412.1828.

[44] S. Alioli, P. Nason, C. Oleari, and E. Re, "NLO single-top production matched with shower in POWHEG: s- and t-channel contributions", *JHEP* **09** (2009) 111, doi:10.1007/JHEP02(2010)011, 10.1088/1126-6708/2009/09/111, arXiv:0907.4076. [Erratum: JHEP02,011(2010)].

[45] S. Frixione, P. Nason, and G. Ridolfi, "A Positive-weight next-to-leading-order Monte Carlo for heavy flavour hadroproduction", *JHEP* **09** (2007) 126, doi:10.1088/1126-6708/2007/09/126, arXiv:0707.3088.

[46] M. Aliev et al., "HATHOR: HAdronic Top and Heavy quarks crOss section calculatoR", *Comput. Phys. Commun.* **182** (2011) 1034–1046, doi:10.1016/j.cpc.2010.12.040, arXiv:1007.1327.

[47] P. Kant et al., "HatHor for single top-quark production: Updated predictions and uncertainty estimates for single top-quark production in hadronic collisions", *Comput. Phys. Commun.* **191** (2015) 74–89, doi:10.1016/j.cpc.2015.02.001, arXiv:1406.4403.

[48] M. Czakon and A. Mitov, "Top++: a program for the calculation of the top-pair cross-section at hadron colliders", *Comput. Phys. Commun.* **185** (2014) 2930, doi:10.1016/j.cpc.2014.06.021, arXiv:1112.5675.

[49] E. Re, "Single-top Wt-channel production matched with parton showers using the POWHEG method", *Eur. Phys. J. C* **71** (2011) 1547, doi:10.1140/epjc/s10052-011-1547-z, arXiv:1009.2450.

[50] N. Kidonakis, "Two-loop soft anomalous dimensions for single top quark associated production with a W- or H-", *Phys. Rev. D* **82** (2010) 054018, doi:10.1103/PhysRevD.82.054018, arXiv:1005.4451.

[51] N. Kidonakis, "NNLL threshold resummation for top-pair and single-top production", *Phys. Part. Nucl.* **45** (2014) 714–722, doi:10.1134/S1063779614040091, arXiv:1210.7813.

[52] H. B. Hartanto, B. Jager, L. Reina, and D. Wackeroth, "Higgs boson production in association with top quarks in the POWHEG BOX", *Phys. Rev. D* **91** (2015) 094003, doi:10.1103/PhysRevD.91.094003, arXiv:1501.04498.

[53] J. Alwall et al., "The automated computation of tree-level and next-to-leading order differential cross sections, and their matching to parton shower simulations", *JHEP* **07** (2014) 079, doi:10.1007/JHEP07(2014)079, arXiv:1405.0301.

[54] R. Gavin, Y. Li, F. Petriello, and S. Quackenbush, "FEWZ 2.0: A code for hadronic Z production at next-to-next-to-leading order", *Comput. Phys. Commun.* **182** (2011) 2388, doi:10.1016/j.cpc.2011.06.008, arXiv:1011.3540.

[55] M. V. Garzelli, A. Kardos, C. G. Papadopoulos, and Z. Trocsanyi, "$t\bar{t}W^{\pm}$ and $t\bar{t}Z$ hadroproduction at NLO accuracy in QCD with parton shower and hadronization effects", *JHEP* **11** (2012) 056, doi:10.1007/JHEP11(2012)056, arXiv:1208.2665.

[56] S. Frixione et al., "Electroweak and QCD corrections to top-pair hadroproduction in association with heavy bosons", *JHEP* **06** (2015) 184, doi:10.1007/JHEP06(2015)184, arXiv:1504.03446.

[57] T. Sjöstrand et al., "An introduction to PYTHIA 8.2", *Comput. Phys. Commun.* **191** (2015) 159, doi:10.1016/j.cpc.2015.01.024, arXiv:1410.3012.

[58] P. Skands, S. Carrazza, and J. Rojo, "Tuning PYTHIA 8.1: the Monash 2013 tune", *Eur. Phys. J. C* **74** (2014) 3024, doi:10.1140/epjc/s10052-014-3024-y, arXiv:1404.5630.

[59] CMS Collaboration, "Event generator tunes obtained from underlying event and multiparton scattering measurements", *Eur. Phys. J. C* **76** (2016) 155, doi:10.1140/epjc/s10052-016-3988-x, arXiv:1512.00815.

[60] CMS Collaboration, "Extraction and validation of a new set of CMS PYTHIA8 tunes from underlying-event measurements", *Eur. Phys. J. C* **80** (2020) 4, doi:10.1140/epjc/s10052-019-7499-4, arXiv:1903.12179.

[61] NNPDF Collaboration, "Parton distributions for the LHC Run II", *JHEP* **04** (2015) 040, doi:10.1007/JHEP04(2015)040, arXiv:1410.8849.

[62] NNPDF Collaboration, "Parton distributions from high-precision collider data", *Eur. Phys. J. C* **77** (2017) 663, doi:10.1140/epjc/s10052-017-5199-5, arXiv:1706.00428.

[63] J. Alwall et al., "Comparative study of various algorithms for the merging of parton showers and matrix elements in hadronic collisions", *Eur. Phys. J. C* **53** (2008) 473, doi:10.1140/epjc/s10052-007-0490-5, arXiv:0706.2569.

[64] R. Frederix and S. Frixione, "Merging meets matching in MC@NLO", *JHEP* **12** (2012) 061, doi:10.1007/JHEP12(2012)061, arXiv:1209.6215.

[65] GEANT4 Collaboration, "GEANT4: A Simulation toolkit", *Nucl. Instrum. Meth. A* **506** (2003) 250–303, doi:10.1016/S0168-9002(03)01368-8.

[66] W. Beenakker, R. Hopker, M. Spira, and P. M. Zerwas, "Squark and gluino production at hadron colliders", *Nucl. Phys. B* **492** (1997) 51, doi:10.1016/S0550-3213(97)80027-2, arXiv:hep-ph/9610490.

[67] A. Kulesza and L. Motyka, "Threshold resummation for squark-antisquark and gluino-pair production at the LHC", *Phys. Rev. Lett.* **102** (2009) 111802, doi:10.1103/PhysRevLett.102.111802, arXiv:0807.2405.

[68] A. Kulesza and L. Motyka, "Soft gluon resummation for the production of gluino-gluino and squark-antisquark pairs at the LHC", *Phys. Rev. D* **80** (2009) 095004, doi:10.1103/PhysRevD.80.095004, arXiv:0905.4749.

[69] W. Beenakker et al., "Soft-gluon resummation for squark and gluino hadroproduction", *JHEP* **12** (2009) 041, doi:10.1088/1126-6708/2009/12/041, arXiv:0909.4418.

[70] W. Beenakker et al., "Squark and Gluino Hadroproduction", *Int. J. Mod. Phys. A* **26** (2011) 2637, doi:10.1142/S0217751X11053560, arXiv:1105.1110.

[71] C. Borschensky et al., "Squark and gluino production cross sections in pp collisions at $\sqrt{s}$ = 13, 14, 33 and 100 TeV", *Eur. Phys. J. C* **74** (2014) 3174, doi:10.1140/epjc/s10052-014-3174-y, arXiv:1407.5066.

[72] W. Beenakker et al., "NNLL resummation for squark-antisquark pair production at the LHC", *JHEP* **01** (2012) 076, doi:10.1007/JHEP01(2012)076, arXiv:1110.2446.

[73] W. Beenakker et al., "Towards NNLL resummation: hard matching coefficients for squark and gluino hadroproduction", *JHEP* **10** (2013) 120, doi:10.1007/JHEP10(2013)120, arXiv:1304.6354.

[74] W. Beenakker et al., "NNLL resummation for squark and gluino production at the LHC", *JHEP* **12** (2014) 023, doi:10.1007/JHEP12(2014)023, arXiv:1404.3134.

[75] W. Beenakker et al., "NNLL-fast: predictions for coloured supersymmetric particle production at the LHC with threshold and Coulomb resummation", *JHEP* **12** (2016) 133, doi:10.1007/JHEP12(2016)133, arXiv:1607.07741.

[76] W. Beenakker et al., "Stop production at hadron colliders", *Nucl. Phys. B* **515** (1998) 3, doi:10.1016/S0550-3213(98)00014-5, arXiv:hep-ph/9710451.

[77] W. Beenakker et al., "Supersymmetric top and bottom squark production at hadron colliders", *JHEP* **08** (2010) 098, doi:10.1007/JHEP08(2010)098, arXiv:1006.4771.

[78] W. Beenakker et al., "NNLL resummation for stop pair-production at the LHC", *JHEP* **05** (2016) 153, doi:10.1007/JHEP05(2016)153, arXiv:1601.02954.

[79] CMS Collaboration, "The fast simulation of the CMS detector at LHC", *J. Phys. Conf. Ser.* **331** (2011) 032049, doi:10.1088/1742-6596/331/3/032049.

[80] A. Giammanco, "The Fast Simulation of the CMS Experiment", *J. Phys. Conf. Ser.* **513** (2014) 022012, doi:10.1088/1742-6596/513/2/022012.

[81] CMS Collaboration, "Particle-flow reconstruction and global event description with the CMS detector", *JINST* **12** (2017) P10003, doi:10.1088/1748-0221/12/10/P10003, arXiv:1706.04965.

[82] CMS Collaboration, "Performance of electron reconstruction and selection with the CMS detector in proton-proton collisions at $\sqrt{s} = 8$ TeV", *JINST* **10** (2015) P06005, doi:10.1088/1748-0221/10/06/P06005, arXiv:1502.02701.

[83] CMS Collaboration, "Performance of CMS muon reconstruction in pp collision events at $\sqrt{s} = 7$ TeV", *JINST* **7** (2012) P10002, doi:10.1088/1748-0221/7/10/P10002, arXiv:1206.4071.

[84] CMS Collaboration, "Identification of heavy-flavour jets with the CMS detector in pp collisions at 13 TeV", *JINST* **13** (2018) P05011, doi:10.1088/1748-0221/13/05/P05011, arXiv:1712.07158.

[85] CMS Collaboration, "Performance of missing transverse momentum reconstruction in proton-proton collisions at $\sqrt{s} = 13$ TeV using the CMS detector", *JINST* **14** (2019) P07004, doi:10.1088/1748-0221/14/07/P07004, arXiv:1903.06078.

[86] M. Burns, K. Kong, K. T. Matchev, and M. Park, "Using subsystem M_{T2} for complete mass determinations in decay chains with missing energy at hadron colliders", *JHEP* **03** (2009) 143, doi:10.1088/1126-6708/2009/03/143, arXiv:0810.5576.

[87] C. G. Lester and B. Nachman, "Bisection-based asymmetric M_{T2} computation: a higher precision calculator than existing symmetric methods", *JHEP* **03** (2015) 100, doi:10.1007/JHEP03(2015)100, arXiv:1411.4312.

[88] CMS Collaboration, "Jet energy scale and resolution in the CMS experiment in pp collisions at 8 TeV", *JINST* **12** (2017) P02014, doi:10.1088/1748-0221/12/02/P02014, arXiv:1607.03663.

[89] CMS Collaboration, "Measurement of top quark pair production in association with a Z boson in proton-proton collisions at $\sqrt{s} = 13$ TeV", *JHEP* **03** (2020) 056, doi:10.1007/JHEP03(2020)056, arXiv:1907.11270.

[90] CMS Collaboration, "CMS luminosity measurement for the 2016 data taking period", CMS Physics Analysis Summary CMS-PAS-LUM-17-001, CMS Collaboration, 2017.

[91] CMS Collaboration, "CMS luminosity measurement for the 2017 data taking period", CMS Physics Analysis Summary CMS-PAS-LUM-17-004, CMS Collaboration, 2017.

[92] CMS Collaboration, "CMS luminosity measurement for the 2018 data-taking period at $\sqrt{s} = 13$ TeV", CMS Physics Analysis Summary CMS-PAS-LUM-18-002, CMS Collaboration, Geneva, 2019.

[93] J. Butterworth et al., "PDF4LHC recommendations for LHC Run II", *J. Phys. G* **43** (2016) 023001, doi:10.1088/0954-3899/43/2/023001, arXiv:1510.03865.

[94] S. Catani, D. de Florian, M. Grazzini, and P. Nason, "Soft gluon resummation for Higgs boson production at hadron colliders", *JHEP* **07** (2003) 028, doi:10.1088/1126-6708/2003/07/028, arXiv:hep-ph/0306211.

[95] M. Cacciari et al., "The $\mathrm{t\bar{t}}$ cross-section at 1.8 TeV and 1.96 TeV: a study of the systematics due to parton densities and scale dependence", *JHEP* **04** (2004) 068, doi:10.1088/1126-6708/2004/04/068, arXiv:hep-ph/0303085.

[96] A. Kalogeropoulos and J. Alwall, "The SysCalc code: A tool to derive theoretical systematic uncertainties", arXiv:1801.08401.

[97] G. Cowan, K. Cranmer, E. Gross, and O. Vitells, "Asymptotic formulae for likelihood-based tests of new physics", *Eur. Phys. J. C* **71** (2011) 1554, doi:10.1140/epjc/s10052-011-1554-0, arXiv:1007.1727. [Erratum: doi:10.1140/epjc/s10052-013-2501-z].

[98] T. Junk, "Confidence level computation for combining searches with small statistics", *Nucl. Instr. Meth. A* **434** (1999) 435, doi:10.1016/S0168-9002(99)00498-2, arXiv:hep-ex/9902006.

[99] A. L. Read, "Presentation of search results: the CL_s technique", *J. Phys. G* **28** (2002) 2693, doi:10.1088/0954-3899/28/10/313.